Atomic structure and diffusion in $Cu_{60}Zr_{40}$ metallic liquid and glass: molecular dynamics simulations

Yong Li Sun,[1] Jun Shen,[1,a)] and Ariel A. Valladares[2]
[1]*State Key Laboratory of Advanced Welding Production Technology, School of Materials Science and Engineering, Harbin Institute of Technology, Harbin 150001, China and Key Laboratory of Micro-Systems and Micro-Structure Manufacturing, Ministry of Education, China*
[2]*Instituto de Investigaciones en Materiales, Universidad Nacional Autónoma de México, Mexico D. F. 04510, Mexico*

(Received 18 April 2009; accepted 12 September 2009; published online 14 October 2009)

Temperature effects on the structural evolution and diffusivity of $Cu_{60}Zr_{40}$ in the liquid and glassy states were studied by molecular dynamics simulations using the Finnis–Sinclair potential. The pair distribution functions and common-neighbor analysis were used to investigate the structural variations. It is found that the amount of pentagonal bipyramids increases sharply in a short temperature range of about 200 K above the glass transition temperature T_g, leading to the increasing of the icosahedral cluster centered by Cu atom and larger Kasper polyhedral cluster centered by Zr atom. The mean square displacement and the self part of the van Hove function were calculated to evaluate the relaxation and transport properties. The cage effect is found to appear at 1100 K. The mode-coupling theory equation is more suitable than the Vogel–Fulcher–Tammann equation to describe the change in diffusivity in the liquid state. The critical temperature T_c, a predicted glass transition temperature in mode-coupling theory, for $Cu_{60}Zr_{40}$ glass former is 1008.2 K. At temperatures near T_c, there is a dynamic crossover. In supercooled liquid state, the dynamic heterogeneity is detected. The comparison of the activation enthalpies of the two components shows that the small atoms transport faster obeying the size effect. © *2009 American Institute of Physics*. [doi:10.1063/1.3245324]

I. INTRODUCTION

Glass transitions take place when liquids are cooled down with a sufficiently high cooling rate. Above the glass transition temperature T_g diffusion drops drastically upon cooling and deviates from the prediction of the Arrhenius equation.[1,2] The diffusion mechanisms in metallic glasses (MGs) are completely different from those in crystalline metals. Collective hopping processes involving a large number of atoms are found to exist in both the glassy state and the liquid state.[2–5] Understanding the mechanisms governing the slowing down of the liquid relaxation is one of the main questions in modern condensed-matter physics.[6–12] The mode-coupling theory (MCT),[13,14] the most advanced glass transition theory, predicts a microscopic glass transition temperature T_c, which is always above the caloric glass transition temperature T_g and usually below the freezing temperature. At this temperature, the atom is trapped by the cage formed by its neighboring atoms. As a result of this cage effect, liquidlike viscous flow vanishes below T_c, and the diffusion proceeds exclusively via activation hopping processes. In MGs, simulations of the $Co_{1-x}Zr_x$ system[15] show that T_c varies significantly with the concentration; but similar investigations in other systems on the concentration dependence of T_c are rare. In the Cu–Zr system, the T_c for $Cu_{33}Zr_{67}$ is reported to be 1025 K,[16] but values for other concentrations are scarce.

Recently, the atomic structures of binary systems have been widely studied by simulations.[17–19] The microscopic structure of the $Cu_{60}Zr_{40}$ MG has been studied experimentally,[20] the first peak positions of the partial pair correlation functions and the nearest-neighbor coordination numbers (CNs) were obtained while other structural details were not studied. The structure of MGs is generally believed to have short-range order instead of long-range order. In our previous study on the $Cu_{60}Zr_{40}$ MG,[21] interpenetrating and face-sharing icosahedra are found to be dominant at 400 K. But how the icosahedral ordering develops in liquid and glassy $Cu_{60}Zr_{40}$ upon cooling is not clear.

In this work, the structural evolution and diffusion in $Cu_{60}Zr_{40}$ metallic liquid and glass are investigated by molecular dynamics (MD) simulations using the LAMMPS code[22] and the Finnis–Sinclair (FS) potential,[23] a potential commonly used for transition metals. The pair distribution function (PDF) and common-neighbor analyses are used to investigate the structural evolution. The mean square displacement (MSD) and the diffusion coefficient D are calculated to evaluate the relaxation and transport properties. The purpose of this paper is to demonstrate the development of short-range order and the diffusion properties in the metallic liquid and glass. The results are expected to shed light on the understanding of the glass transition in these metallic systems.

II. SIMULATION AND ANALYSIS METHODS

In the present study, the FS potential was adopted to simulate $Cu_{60}Zr_{40}$ metallic liquid and glass. The total energy of this interatomic potential has the form

a)Author to whom correspondence should be addressed. Electronic mail: junshen@hit.edu.cn.

$$E_i = F_\alpha\left[\sum_{j\neq i}\rho_{\alpha\beta}(r_{ij})\right] + \frac{1}{2}\sum_{j\neq i}\phi_{\alpha\beta}(r_{ij}),$$

where α and β are the types of atomic elements, r_{ij} is the interatomic distance between atoms i and j, $\phi_{\alpha\beta}(r_{ij})$ is the two-body potential, F is the embedding energy, and $\rho_{\alpha\beta}(r_{ij})$ is the electron density function. This type of potential has been used to model the structure and elastic properties of Cu–Zr alloys.[24,25]

MD simulations were performed on a cubic box with 1269 atoms involving 756 Cu atoms and 513 Zr atoms under three-dimensional periodic boundary conditions. The constant pressure and temperature NPT ensemble was used and controlled with the Nosé–Hoover algorithm.[26] The initial density of the alloy was taken as 7.53 gcm^{-3}, corresponding to the reported experimental value.[20] The system was designed to be melted and equilibrated at 1800 K for 200 ps under the pressure of 0 Pa, then cooled down to 400 K with three different cooling rates of 2.5×10^{13}, 2.5×10^{12}, and 2.5×10^{11} Ks^{-1} to test the effect of cooling rate on the T_g. The integration time step was taken as 1 fs, a value sufficiently small to reduce the fluctuations of the total energy. Simulations of 500 ps were carried out after equilibration for 200 ps for every 100 K to collect the corresponding properties, then the conjugate gradient algorithm was used to obtain the inherent structure, in which random configurations corresponding to the selected temperatures were extracted for structural analysis.

The PDF presents the information of the local atomic structure and is frequently used in the investigation of noncrystalline systems. This function is defined as

$$g(r) = \frac{1}{N}\sum_{ij}\delta(r - r_{ij}),$$

where N is the number of atoms in the simulation box. The PDF shows the probability of finding another atom at a distance r from an origin atom.

The MSD is given as

$$\langle r^2(t)\rangle = \frac{1}{N}\sum_{i=1}^{N}\langle|r_i(t) - r_i(0)|^2\rangle,$$

where $r_i(t)$ is the atomic position at time t, and $\langle\ldots\rangle$ the ensemble average.

The diffusion coefficient D can be calculated from the long-time evolution of the MSDs,

$$D^l(T) = \lim_{t\to\infty}\frac{1}{6}\partial_t\langle r^2(t)\rangle^l,$$

where l denotes the atoms Cu or Zr.

III. RESULTS AND DISCUSSION

Upon cooling, average atomic volume, a parameter described by the ratio of volume of the system to number of atoms, is generally used to evaluate the density variation in the system studied. Figure 1 shows the average atomic volume V of the alloy $Cu_{60}Zr_{40}$ during the cooling processes with the three cooling rates of 2.5×10^{13}, 2.5×10^{12}, and 2.5×10^{11} Ks^{-1}. The change in the slope of the average atomic volume indicates the glass transition of this alloy for the three cases studied. The slight difference in the three curves implies that the average atomic volume is insensitive to the cooling rate in the given cooling-rate range, in agreement with previous calculations.[16] The intersection of the extrapolations for curves representing the supercooled melt and the glass denotes the glass transition temperature, T_g. As is well known, the T_g is not fixed but depends on the thermal history. In the present simulation the values of T_g of the $Cu_{60}Zr_{40}$ MG for the cooling rates of 2.5×10^{13}, 2.5×10^{12}, and 2.5×10^{11} Ks^{-1} are 907, 946, and 942 K, respectively, all are higher than the experimental value of 711 K.[20] The systematic cooling-rate dependence of T_g is not obvious in our simulations. In what follows, the system obtained with the highest cooling rate 2.5×10^{13} Ks^{-1} will be discussed in detail.

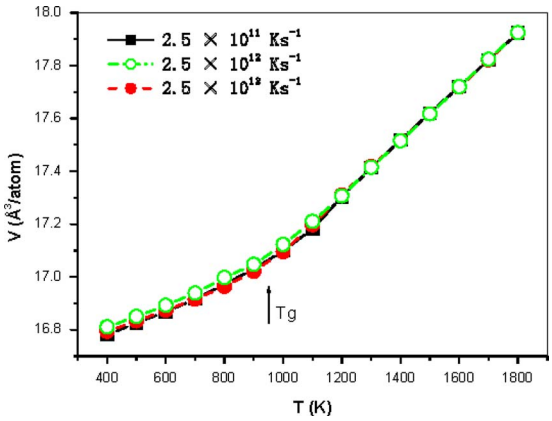

FIG. 1. (Color online) Average atomic volumes V as a function of temperature for the $Cu_{60}Zr_{40}$ alloy for the three cooling rates: 2.5×10^{13}, 2.5×10^{12}, and 2.5×10^{11} Ks^{-1}.

Figure 2 shows the partial PDFs (pPDF) $g(r)$ of the alloy $Cu_{60}Zr_{40}$ at temperature intervals of 100 K between 1800 and 400 K. In the three groups of plots corresponding to Cu–Cu, Cu–Zr, and Zr–Zr pairs, the first peaks increase in height and decrease in width upon cooling, indicating that the structures become more condensed as the temperature lowers. Splitting of the second peaks can be observed in the Cu–Cu and Cu–Zr pairs as the temperature decreases and the first subpeaks grow higher than the second ones. The splitting of the second peaks for the Cu–Cu and Cu–Zr pairs at lower temperatures gives further evidence of the formation of the $Cu_{60}Zr_{40}$ undercooled liquid and glass.[27] The increase in the heights of the two subpeaks indicates that the atoms rearrange in a more orderly fashion upon cooling. For the case of the Zr–Zr pair, no split is found in the second peak but a shift in the second peak position to the left and an increase in height during the cooling process appear. This reveals that the local environments of the Cu and Zr atoms are different in the $Cu_{60}Zr_{40}$ metallic liquid and glass.

The position of the first peak in the PDF denotes the most probable first-neighbor bond length. Figure 2 shows that the positions of the first peaks remain nearly unchanged upon cooling. The first peak positions derived from the present work and those obtained from experiment[20,28] are

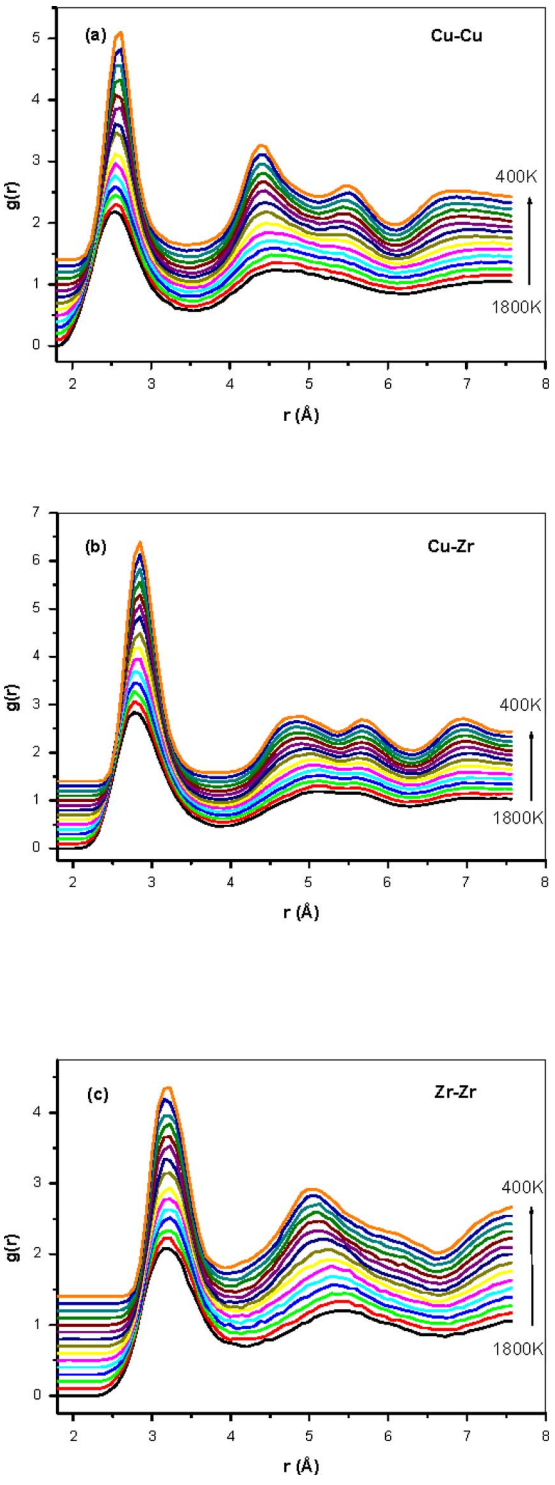

FIG. 2. (Color online) pPDFs g(r) for the $Cu_{60}Zr_{40}$ alloy in the temperature range from 1800 K to 400 K at an interval of 100 K. (a) Cu–Cu pair, (b) Cu–Zr pair, and (c) Zr–Zr pair.

listed in Table I. It should be noted that the cooling rates are significantly different due to the different processes. The calculated first-neighbor bond lengths are consistent with the corresponding experimental values, indicating that the FS potential used herein is suitable to describe the structure of the $Cu_{60}Zr_{40}$ metallic liquid and glass.

The CN is used in structural studies to provide a statistical description of the nearest-neighbor atoms in liquid and

TABLE I. Experimental and simulated first peak positions r for the $Cu_{60}Zr_{40}$ alloy.

	r_{Cu-Cu} (Å)	r_{Cu-Zr} (Å)	r_{Zr-Zr} (Å)
XRD[a]	···	2.73	3.13
EXAFS[b]	2.52	2.69	3.15
MD[c]	2.54	2.85	3.23

[a]Reference 20.
[b]Reference 28.
[c]This work.

amorphous systems. The partial CNs z_{ii} and z_{ij}, corresponding to the i-i and i-j pairs, respectively, are calculated by integrating the first peaks of the pPDFs to the first minima, and the total CNs z_i for the i atoms can be estimated by means of $z_i = z_{ii} + z_{ij}$. Figure 3 shows the partial and total CNs z as a function of temperature for the present alloy $Cu_{60}Zr_{40}$. Insignificant variations in the nearest-neighbor CNs upon cooling indicate that the average CN is temperature independent. Thus upon cooling the number of atoms in the first shell is nearly unchanged but the atoms arrange themselves more orderly as the formation of a structure with fivefold symmetry described below. This result is in good agreement with previous simulation result for $Cu_{46}Zr_{54}$ MG.[29] The total CN for a Cu atom is about 11.8 with 5.67 Cu atoms and 6.17 Zr atoms around it. For the case of Zr, the total CN is about 15 involving 9.25 Cu atoms and 5.75 Zr atoms. These results suggest that in the first shell, the central Cu atom is surrounded by two subshells, one with 5.67 Cu atoms at an average distance of 2.54 Å (Cu–Cu bond length) and 6.17 Zr atoms at an average distance of 2.85 Å (Cu–Zr bond length). Thus the average composition of the clusters centered by Cu is $Cu_{6.67}Zr_{6.17}$, close to Cu_7Zr_6. For the central Zr atom, the two subshells are 9.25 Cu and 5.75 Zr at average distances of 2.85 and 3.23 Å (Zr–Cu and Zr–Zr bond lengths), respectively. Therefore the Zr-centered cluster is $Cu_{9.25}Zr_{6.75}$ on average, close to Cu_9Zr_7, a larger cluster than the Cu-centered cluster due to the fact that the atomic radius of the central Zr atom is larger than that of Cu.

As an example, Fig. 4 shows a 13-atom cluster Cu_7Zr_6 centered by Cu atom and a 16-atom cluster Cu_9Zr_7 centered

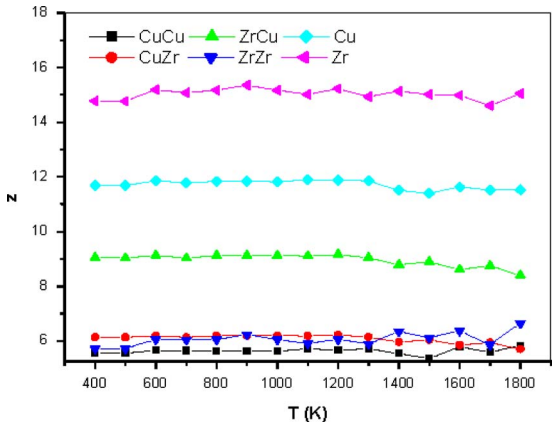

FIG. 3. (Color online) CNs z for the $Cu_{60}Zr_{40}$ alloy as a function of temperature.

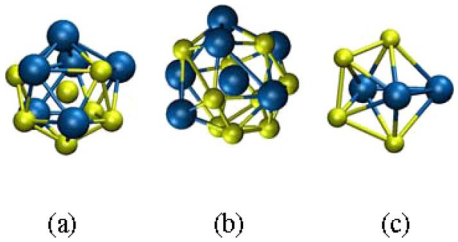

FIG. 4. (Color online) (a) Cu-centered icosahedral cluster with the composition of Cu_7Zr_6, (b) Zr-centered polytetrahedral cluster with the composition of Cu_9Zr_7, and (c) a pentagonal bipyramid derived from a random configuration at 400 K. The blue and yellow balls denote Zr and Cu atoms, respectively. The connecting bars represent the bonds between the surrounding atoms within the first nearest-neighbor distance.

by Zr atom obtained from a configuration at 400 K. It is to be noted that, besides the Cu_7Zr_6 and Cu_9Zr_7, there are many other types of clusters with different numbers of atoms or space distributions in any configuration upon cooling, resulting in the structural complication of the $Cu_{60}Zr_{40}$ alloy.

To evaluate the coordination tendency of the Cu and Zr atoms in $Cu_{60}Zr_{40}$, the Cowley chemical short-range order parameter (CSRO) for the nearest neighboring shell is calculated as[30,31]

$$\alpha_{ij} = 1 - z_{ij}/c_j(z_{ii} + z_{ij}),$$

where c_j is the concentration of particle j and z_{ij} is the number of particle j around a particle i within a sphere of radius R_{ij}. For random atomic distribution, the value of α_{ij} is zero. The positive and negative values of α_{ij} indicate a preference for like-neighbor and unlike-neighbor bonds, respectively. The calculated CSRO parameters for alloy $Cu_{60}Zr_{40}$ are displayed in Fig. 5. Negative values for α_{CuZr} are found in the whole temperature range studied indicating that unlike-neighbor bonding is more likely to occur in this alloy. This result is consistent with the PDF data where the first peak of the Cu–Zr pRDF is higher than those of Cu–Cu and Zr–Zr.

The topological SRO is analyzed using the common-neighbor analysis,[32] which serves as a decomposition of the radial distribution function according to the environment of the pairs. In this method, a sequence of three indices, jkl, is used to characterize the local environment of the pair. The first index, j, denotes the number of neighbors common to

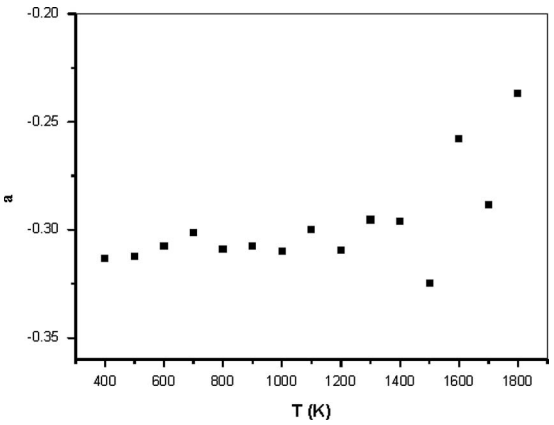

FIG. 5. Chemical short-range order parameter α as a function of temperature.

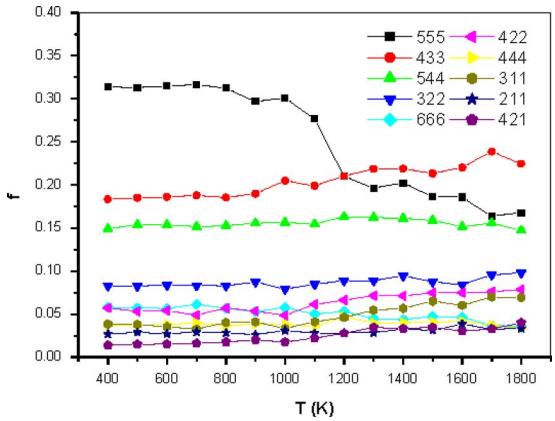

FIG. 6. (Color online) Normalized fraction of CN pairs f in the $Cu_{60}Zr_{40}$ alloy as a function of temperature upon cooling at the rate of 2.5×10^{13} Ks^{-1}.

both atoms. The second index, k, denotes the number of bonds between these common neighbors and the third index, l, is the number of bonds in the longest continuous chain among the k common neighbors. Different common-neighbor pairs are associated with different local structures. For instance, the index 555 is characteristic of icosahedral order, while 433 and 544 are characteristic of defect icosahedral structure, and 421 and 422 are characteristic of fcc and hcp structure. The only bonded pairs in the fcc crystal are 421, while the hcp crystal has equal numbers of 422 and 421. The 666 and 444 pairs are related to a bcc crystal. The 311 pair represents the rhombus symmetrical feature of the short-range order.

The normalized fractions of common-neighbor pairs f as a function of temperature are given in Fig. 6. The results show that the pairs in the majority are 555, 433, and 544 pairs, indicating the dominance of icosahedral packing due to a more favorable energy.[33] The presence of small fractions of 422 and 421 pairs denotes insignificant crystalline short-range order. Percentages of other pairs (including 322, 666, 444, 311, and 211) are low. It is found that the structural evolution of alloy $Cu_{60}Zr_{40}$ upon cooling can be divided into three stages according to the change in the amount of 555 pairs because of its relatively larger change than those of other pairs. Above 1200 K, the 555 pair fraction increases slowly from 16.3% to 20.9% with the decrease in temperature, and then between 1200 and 1000 K, this fraction increases sharply from 20.9% to 30.1%, while below 1000 K, that is, in the glassy state, the 555 pair fraction nearly remains invariable with a value of about 31%. Therefore, the amount of pentagonal bipyramids, as shown in Fig. 4(c), develops slowly upon cooling above 1200 K, and in the second stage, grows rapidly within a short temperature range above T_g. As evolving into the glassy state, the amount of pentagonal bipyramids remains nearly unchanged. Considering that in the $Cu_{60}Zr_{40}$ metallic liquid and glass, the Cu and Zr atoms are evenly mixed, the pentagonal bipyramids might involve any possible combination of seven Cu and Zr atoms and this partly reveals the diversity of the local structure. The appearance and growth of the pentagonal bipyramid illuminates that the atomic arrangement tends to form the fivefold

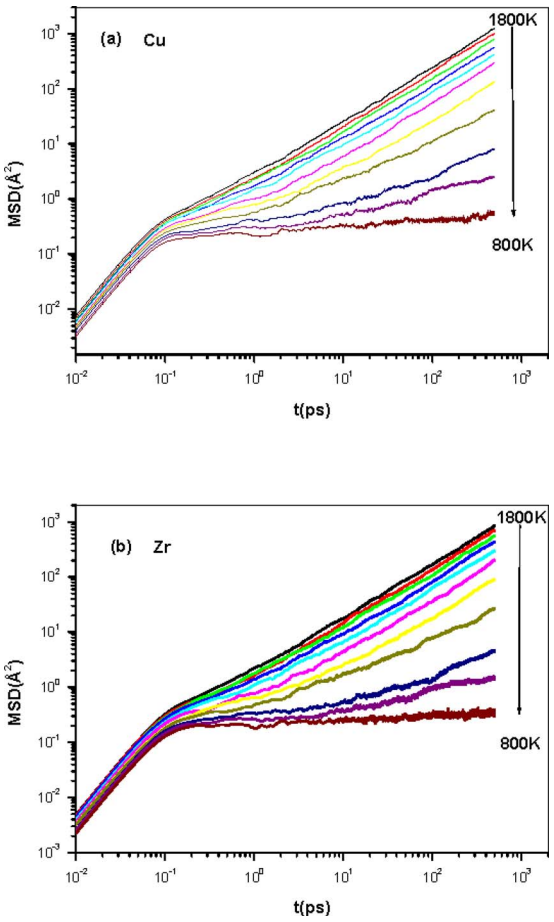

FIG. 7. (Color online) A log-log plot of the time dependence of the MSD for Cu (a) and Zr (b) in the $Cu_{60}Zr_{40}$ alloy at the cooling rate of 2.5×10^{13} Ks^{-1}. Temperatures vary from 1800 K (the top line) to 800 K (the bottom line).

symmetry, characteristic of icosahedral cluster. Thus the icosahedral clusters will increase in number with the evolution of pentagonal bipyramids and are mainly centered by Cu atoms, as shown in Fig. 4(a), as the average CN of Cu atom is close to 12. The sharp increase in icosahedral clusters in liquid state well above T_g improves the liquid stability and in turn enhances the glass forming ability of the $Cu_{60}Zr_{40}$ alloy. As for Zr atoms, they will form larger Kasper polytehedral cluster, as shown in Fig. 4(b), because of its large average CN of 15.

The MSD of the Cu and the Zr atoms are calculated for metallic liquid and glass $Cu_{60}Zr_{40}$ and plotted against time, as shown in Fig. 7. At a short time (less than 0.1 ps), an increment in MSD proportional to t^2 is observed which is due to the vibrations and ballistic motion. With the lowering of temperature MSD decreases slightly. For a longer time (more than 10 ps), MSD increases proportionally to t at temperatures higher than 1200 K, indicating the long-range diffusion which is typical for a simple liquid. At an intermediate period of time (0.1–10 ps), a plateau appears and becomes pronounced when the temperature is lowered below 1100 K. The approaching and the subsequent departure from the plateau defines the β-relaxation regime as described by the MCT. The appearance of the plateau is caused by the cage effect; it takes time for an atom to escape from the "cage"

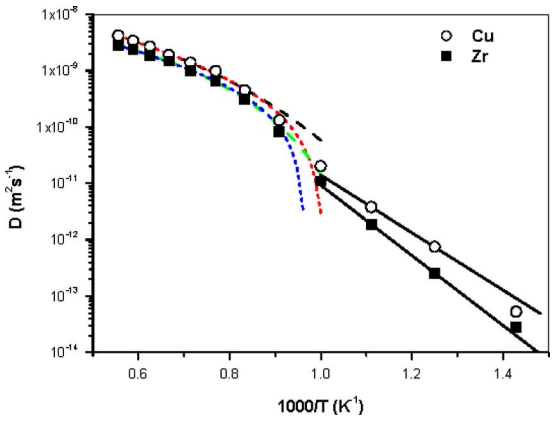

FIG. 8. (Color online) Arrhenius plots of the diffusion coefficients D for $Cu_{60}Zr_{40}$ metallic liquid and glass. The long dashed lines, short dashed lines and solid lines are the VFT fits, the power-law fits and the linear fits, respectively.

formed by its surrounding neighbors.[7] The lower the temperature, the longer the time required for escape, thus the more distinct the plateau. In the glass state, at a temperature below 800 K, the atoms are trapped in the cages and no long-range diffusion is found on the time scale studied. Similar results for tests of MCT have been reported elsewhere.[34]

Figure 8 shows the temperature dependence of the self-diffusion coefficients D for Cu and Zr in both the liquid state and the glassy state. The results presented are obtained for temperatures above 700 K, because at low temperatures meaningful calculations are unattainable due to the very small atomic mobility. It is found that the diffusion coefficient of Cu is larger than that of Zr, which is due to the fact that the Cu atom has a smaller atomic radius and a smaller mass. At temperatures above T_g, both curves show nonlinear Arrhenius behavior, i.e., the effective activation enthalpy $-k_B \partial \ln D / \partial T^{-1}$ increases upon cooling, which is attributed to the incomplete relaxation to the metastable equilibrium state at these temperatures.

The diffusion coefficients above T_g are fitted by the power-law expression predicted in the MCT

$$D^l(T) \propto |T - T_c|^{\gamma},$$

where T_c is the critical temperature, which is located well above the caloric glass transition temperature T_g and does not depend on the experimental time scale. MCT predicts a purely dynamical phase transition at T_c. It is believed that the mode-coupling temperature marks a crossover between two types of dynamic regimes: one based on single-diffusion and the other on cooperative hopping.[14] The fitting parameters are listed in Table II. It is found that for Cu, $T_c^{Cu}=991$ K, $\gamma_{Cu}=1.6$, and for Zr, $T_c^{Zr}=1034$ K, $\gamma_{Zr}=1.37$. T_c^e for the entire system can be evaluated using the expression $T_c^e = c_{Cu}T_c^{Cu} + c_{Zr}T_c^{Zr}$ and giving the value of 1008.2 K, which is somewhat higher than T_g of the present system and lower than T_c of 1025 K in a previous simulation of $Cu_{33}Zr_{67}$ using the modified embedded atom method.[16] The critical temperature T_c of Cu is smaller than that of Zr, indicating that the smaller atoms (Cu) have a faster relaxation. In our simulation, γ_{Cu} is larger than γ_{Zr}, but in $Cu_{33}Zr_{67}$, the result is reverse, with $\gamma_{Cu}=1.34$ and $\gamma_{Zr}=1.92$.[16] The physical mean-

TABLE II. Diffusivity fitting parameters using the MCT power-law function, the VFT function, and the Arrhenius law.

	Cu[a]	Cu[b]	Zr[a]	Zr[b]
T_c (K)	991	1025	1034	1025
γ	1.6	1.34	1.37	1.92
D_0^{VFT} ($m^2\ s^{-1}$)	4.1×10^{-8}	3.7×10^{-8}	1.43×10^{-8}	2.65×10^{-8}
E^{VFT} (eV)	0.24	0.3	0.15	0.28
T_0 (K)	573.33	477	750.73	641
D_0^{Arrh} ($m^2\ s^{-1}$)	1.72×10^{-6}	1.41×10^{-5}	2×10^{-5}	1.09×10^{-3}
E^{Arrh} (eV)	1.01	1.1	1.23	1.7

[a]This work.
[b]Data in Ref. 16.

ing of the parameter γ is not clear. Diffusion is also fitted by the Vogel–Fulcher–Tammann (VFT) equation

$$D^{\mathrm{VFT}} = D_0^{\mathrm{VFT}} \exp[-E^{\mathrm{VFT}}/k_B(T-T_0)],$$

with the fitting parameters given in Table II. Figure 8 shows that the power-law fits are much better than the VFT fits at temperatures above T_c; therefore the results presented here substantiate the reliability of MCT.

In the glassy state, the diffusivities are fitted by the Arrhenius equation

$$D^{\mathrm{Arrh}} = D_0^{\mathrm{Arrh}} \exp(-E^{\mathrm{Arrh}}/k_BT),$$

where E^{Arrh} is the activation enthalpy. The best fits for the alloy $Cu_{60}Zr_{40}$ are $D_0^{\mathrm{Arrh}}=1.72\times10^{-6}$ $m^2\ s^{-1}$, $E^{\mathrm{Arrh}}=1.01$ eV, for Cu, and $D_0^{\mathrm{Arrh}}=2\times10^{-5}$ $m^2\ s^{-1}$, $E^{\mathrm{Arrh}}=1.23$ eV for Zr, consistent with the values obtained by Kluge *et al.*[16] It is found that the activation enthalpy of Cu is smaller than Zr, indicating that the smaller Cu atoms diffuse faster than the bigger Zr atoms. The size dependence of the activation enthalpy is believed to reflect essential features of the actual diffusion mechanism.[35] Obviously, the activation enthalpy changes significantly near T_c for both Cu and Zr atoms, indicating that there should be a dynamic crossover.[36]

At temperatures above T_c, it is convenient for the atomic motion to be detected by the self part of the van Hove function $G_s(r,t)$ which gives the probability of finding the same atom at a distance r at time t from its origin position at time $t=0$and takes the form

$$G_s(r,t) = \langle 1/N \sum_{i=1}^{N} \delta[r - r_i(t) + r_i(0)] \rangle,$$

where δ(r) is the δ function.[34,37] Figure 9 shows $4\pi r^2 G_s(r,t)$ for $Cu_{60}Zr_{40}$ alloy in liquid state of 1300 K, supercooled liquid state of 1100 K, and glassy state of 900 K. It is found that at 1300 K, the curves broaden and decay regularly as t increases, indicating that, on the average, the atoms travel further with time and hence present a liquidlike flow.

In the supercooled liquid state, $4\pi r^2 G_s(r,t)$ has a Gaussian form to a first approximation but deviates with time increasing, suggesting the presence of dynamical heterogeneities.[38–40] Therefore, at the temperature $T=1100$ K, most of the atoms vibrates near their original positions and are trapped in the cages formed by their neighbor atoms at a time less than 10 ps. Then the amount of atoms diffusing to distances larger than 2.5 Å, the first nearest-neighbor distance for Cu–Cu pairs, gradually increases with time, corresponding to the late β relaxation when the atoms move to the positions on the cages or even further. In the case of glassy state, the deviation of $4\pi r^2 G_s(r,t)$ from the Gaussian form still exists at a time longer than 100 ps, as shown in the inset of Fig. 9(c), revealing that there are still a few atoms escaping from their initial cages. Similar behavior has been found in the experimental measurements for $Co_{1-x}Zr_x$ and $Pd_{40}Cu_{30}Ni_{10}P_{20}$ systems and numerical simulations for Lennard-Jones binary mixture and Al systems.[5,41,34,42]

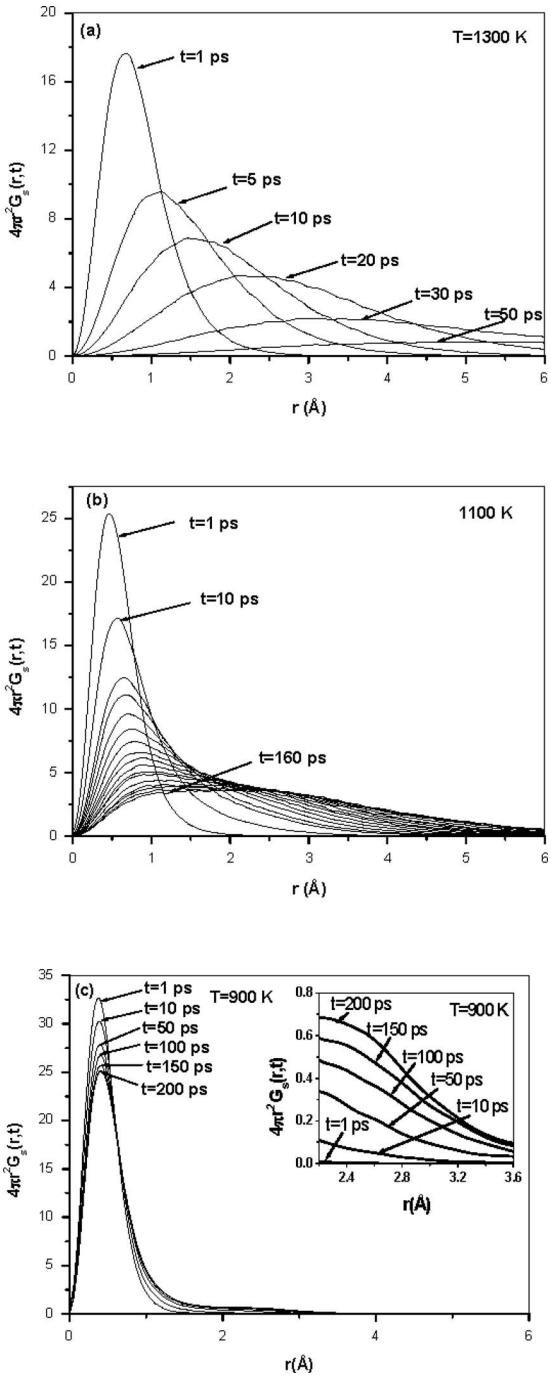

FIG. 9. $4\pi r^2 G_s(r,t)$ as a function of r varying with time. (a) $T=1300$ K, (b) $T=1100$ K, and (c) $T=900$ K. In (b), the time takes $t=1$ ps and $t=10$ n ps with $n=1,2\ldots,16$. The inset in (c) is the enlargement of the curves at 900 K at a distance between 2.2 and 3.6 Å.

Figure 10 shows $4\pi r^2 G_s(r,t)$ for the two component el-

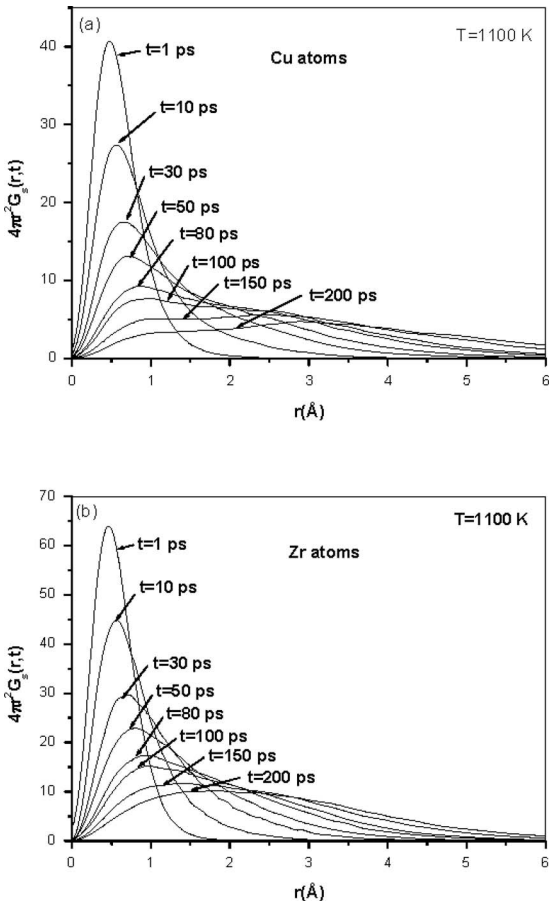

FIG. 10. $4\pi r^2 G_s(r,t)$ for Cu (a) and Zr (b) atoms at 1100 K.

ements Cu and Zr at 1100 K. It can be seen that for Cu atoms, a small peak gradually appears at a distance around 3 Å for a time longer than 80 ps, but for the case of Zr atoms there is no such peak at the same region. The presence of the small peak is believed to be the characteristic of the hopping processes, corresponding to thermally assisted transitions over energy barriers from one potential minimum to another.[34,43,44] Hence for Cu atoms the activated hopping process takes place in the supercooled liquid state, while the case is not true for Zr atoms.

The difference in the dynamics for the two types of atoms is due to the different local environments around them. For Cu atoms, the CNs are relatively small, thus the atoms exist in much smaller local clusters where the interaction forces are weaker and the barrier heights are relatively lower, which is favorable for Cu atoms to achieve the activated process, leading to the larger diffusivity of Cu atoms than that of Zr atoms.

IV. CONCLUSIONS

The atomic structure and the diffusion behaviors of the $Cu_{60}Zr_{40}$ metallic liquid and glass were studied by MD simulations with FS potential. The results reveal that upon cooling, the average first-neighbor bond lengths and first nearest-neighbor CNs approximately remain unchanged, but the atoms arrange themselves more orderly. The amount of pentagonal bipyramids increases sharply in a short temperature range of about 200 K above the glass transition temperature T_g, promoting the growth of icosahedral cluster centered by Cu atom and larger Kasper polyhedral cluster centered by Zr atom. At temperatures above 1200 K, two stages, short-time vibrations and long-time flow, are found in the liquid relaxation. When the temperature is lowered below 1100 K, the cage effect appears on the time scale of the β relaxation. The critical temperature T_c in MCT theory for $Cu_{60}Zr_{40}$ alloy is found to be 1008.2 K. As expected, the small atoms diffuse faster than the larger ones. In the liquid state the MCT power-law equation is more suitable in describing the diffusion kinetics than the VFT equation. At temperatures near T_c, there is a dynamic crossover. At 1100 K, the dynamical heterogeneity is detected. The activated hopping process takes place for Cu atoms but not for Zr atoms.

ACKNOWLEDGMENTS

This work was supported by the National Natural Science Foundation of China (NSFC) under Grant Nos. 50771040 and 10732010, and the Heilongjiang Provincial Natural Science Foundation (Contract No. JC200806).

[1] H. Teichler, Defect Diffus. Forum **143–147**, 717 (1997).
[2] H. Teichler, J. Non-Cryst. Solids **293–295**, 339 (2001).
[3] F. Faupel, P. W. Hüppe, and K. Rätzke, Phys. Rev. Lett. **65**, 1219 (1990).
[4] X. P. Tang, U. Geyer, R. Busch, W. L. Johnson, and Y. Wu, Nature (London) **402**, 160 (1999).
[5] A. Heesemann, V. Zöllmer, K. Rätzke, and F. Faupel, Phys. Rev. Lett. **84**, 1467 (2000).
[6] P. W. Anderson, Science **267**, 1615 (1995).
[7] C. A. Angell, Science **267**, 1924 (1995).
[8] P. G. Debenedetti and F. H. Stillinger, Nature (London) **410**, 259 (2001).
[9] P. Mayer, H. Bissig, L. Berthier, L. Cipelletti, J. P. Garrahan, P. Sollich, and V. Trappe, Phys. Rev. Lett. **93**, 115701 (2004).
[10] G. A. Appignanesi, J. A. Rodrı'guez Fris, R. A. Montani, and W. Kob, Phys. Rev. Lett. **96**, 057801 (2006).
[11] C. Toninelli, M. Wyart, L. Berthier, G. Biroli, and J. P. Bouchaud, Phys. Rev. E **71**, 041505 (2005).
[12] S. Karmakar, C. Dasgupta, and S. Sastry, Proc. Natl. Acad. Sci. U.S.A. **106**, 3675 (2009).
[13] E. Leutheusser, Phys. Rev. A **29**, 2765 (1984).
[14] W. Gotze and L. Sjogren, Rep. Prog. Phys. **55**, 241 (1992).
[15] U. K. Rößler and H. Teichler, Phys. Rev. E **61**, 394 (2000).
[16] M. Kluge and H. R. Schober, Phys. Rev. B **70**, 224209 (2004).
[17] K. P. Tai, N. Gao, X. D. Dai, J. H. Li, and B. X. Liu, J. Appl. Phys. **101**, 124905 (2007).
[18] K. P. Tai, L. T. Wang, and B. X. Liu, J. Appl. Phys. **102**, 124902 (2007).
[19] S. Y. Wang, C. Z. Wang, M. Z. Li, L. Huang, R. T. Ott, M. J. Kramer, D. J. Sordelet, and K. M. Ho, Phys. Rev. B **78**, 184204 (2008).
[20] N. Mattern, A. Schöps, U. Kühn, J. Acker, O. Khvostikova, and J. Eckert, J. Non-Cryst. Solids **354**, 1054 (2008).
[21] Y. L. Sun and J. Shen, J. Non-Cryst. Solids **355**, 1557 (2009).
[22] S. J. Plimpton, J. Comput. Phys. **117**, 1 (1995).
[23] M. W. Finnis and J. E. Sinclair, Philos. Mag. A **50**, 45 (1984).
[24] M. I. Mendelev, D. J. Sordelet, and M. J. Kramer, J. Appl. Phys. **102**, 043501 (2007).
[25] M. I. Mendelev, D. K. Rehbein, R. T. Ott, M. J. Kramer, and D. J. Sordelet, J. Appl. Phys. **102**, 093518 (2007).
[26] S. Nosé, Mol. Phys. **52**, 255 (1984); J. Chem. Phys. **81**, 511 (1984).
[27] G. X. Li, Y. F. Liang, Z. G. Zhu, and C. S. Liu, J. Phys.: Condens. Matter **15**, 2259 (2003).
[28] A. Sadoc, D. Raoux, P. Lagarde, and A. Fontaine, J. Non-Cryst. Solids **50**, 331 (1982); Y. Waseda and H. S. Chen, Phys. Status Solidi **87**, 777 (1978) (b).
[29] G. Duan, D. H. Xu, Q. Zhang, G. Y. Zhang, T. Cagin, W. L. Johnson, and W. A. Goddard III, Phys. Rev. B **71**, 224208 (2005).
[30] M. Asta, D. Morgan, J. J. Hoyt, B. Sadigh, J. D. Althoff, D. de Fontaine, and S. M. Foiles, Phys. Rev. B **59**, 14271 (1999).

[31]J. M. Cowley, Phys. Rev. **77**, 669 (1950).
[32]A. S. Clarke and H. Jónsson, Phys. Rev. E **47**, 3975 (1993).
[33]J. P. K. Doye and D. J. Wales, Science **271**, 484 (1996).
[34]W. Kob and H. C. Andersen, Phys. Rev. E **51**, 4626 (1995).
[35]F. Faupel, W. Frank, M. P. Macht, H. Mehrer, V. Naundorf, K. Rätzke, H. R. Schober, S. K. Sharma, and H. Teichler, Rev. Mod. Phys. **75**, 237 (2003).
[36]H. C. Andersen, Proc. Natl. Acad. Sci. U.S.A. **102**, 6686 (2005).
[37]J. P. Hansen and I. R. McDonald, *Theory of Simple Liquids* (Academic, London, 1986), p. 198.
[38]M. M. Hurley and P. Harrowell, J. Chem. Phys. **105**, 10521 (1996).
[39]W. Kob, C. Donati, S. J. Plimpton, P. H. Poole, and S. C. Glotzer, Phys. Rev. Lett. **79**, 2827 (1997).
[40]R. Candelier, O. Dauchot, and G. Biroli, Phys. Rev. Lett. **102**, 088001 (2009).
[41]V. Zollmer, K. Ratzke, F. Faupel, A. Rehmet, and U. Geyer, Phys. Rev. B **65**, 220201(R) (2002).
[42]M. Li, C. Z. Wang, M. I. Mendelev, and K. M. Ho, Phys. Rev. B **77**, 184202 (2008).
[43]M. Goldstein, J. Chem. Phys. **51**, 3728 (1969).
[44]J. N. Roux, J. L. Barrat, and J. P. Hansen, J. Phys.: Condens. Matter **1**, 7171 (1989).